

Ph.D. Dissertation of Sandeep Gaan, "Scanning Tunneling Spectroscopy of Molecular Thin Films and Semiconductor Nanostructures", Dept. Physics, Carnegie Mellon University, Pittsburgh, Pennsylvania, USA (2008).

## Chapter 3

# STM/STS study of pentacene thin films deposited on SiC

### 3.1 Introduction

Nano-scale study of structural and electronic properties of organic semiconductors promises not only new applications, but also many novel physical phenomena. Among small semiconducting molecules, Pn in particular can be used as a model system for such type of nano-scale studies, especially for understanding electronic and charge transport properties in these small molecular systems in general. In this chapter, we discuss the use of STM/STS to probe nanometer scale electronic properties of Pn thin films and thereby study the problem of charge transport in the films.

There are two major advantages in our experiments on Pn thin films as described below. By ensuring clean UHV conditions for preparation of Pn films on SiC substrates we have eliminated unwanted effects of contamination which has a large effect on electronic properties of Pn. We will discuss effects of oxygen on the tunneling spectra and possible mechanisms in the later part of this chapter. A contamination free Pn film is essential for high quality reproducible results from experiments. The second unique advantage in our experimental method is in the use of the STM probe-tip as an electrode for efficient charge injection into the Pn films. The charge injection problem in Pn, which is relevant for other organic semiconductors as well, is briefly described below. Pentacene, like most other semiconducting molecules, has a low electron affinity value of about 3 eV. Most of the metals used as electrodes have work functions ranging from roughly 4 to 6 eV. Since Pn has a band gap of  $\sim 2$  eV, it is quite clear that the barrier for injecting electrons into the lowest-unoccupied molecular orbital (LUMO) is much higher than that for injecting holes into highest-occupied molecular orbital (HOMO) level. Consequently Pn behaves as a p-type semiconductor, not because of extrinsic doping as in the case of inorganic semiconductors, but because of the relative ease of hole injection into the HOMO level.

Using STM probe-tip for charge injection has two advantages over conventional metal contacts used as cathodes. First, any influence from the metal-semiconductor interface (such as intermixing at the interface) is avoided. Since Pn is quite reactive, the metal contacts can react with the molecules altering the electronic properties of the film considerably. Since STM probe-tip does not make contact in our experiments, we have

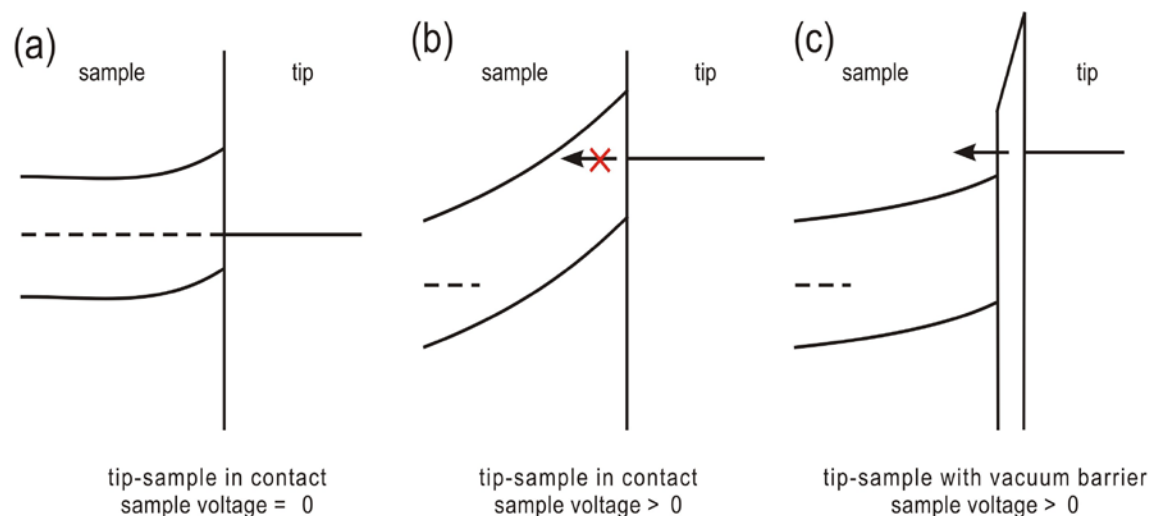


FIGURE 3.1: Schematic energy diagrams comparing situations of tip-sample contact [(a) with zero applied voltage and (b) with positive sample voltage] to tunneling through a vacuum barrier [(c) with positive sample voltage]. Tunneling through vacuum barrier makes LUMO states accessible.

completely eliminated these types of problems due to the metal-semiconductor interface. Secondly, states in the LUMO band become easily accessible by direct injection of electrons into this band. This situation is schematically illustrated in Fig. 3.1, comparing the cases of metal-semiconductor contact [panels (a) and (b)] with a vacuum tunneling barrier [panel (c)]. Under a positive sample bias the barrier height is very high for electrons coming from metal electrode in contact with the sample, Fig. 3.1(b), and states in the LUMO level are not accessible. However for a STM probe-tip most of the applied bias voltage drops in the vacuum junction since the dielectric constant of the semiconductor is large. Since the thickness of the vacuum barrier is quite small ( $\sim 1$  nm), the tunneling probability through the vacuum is large enough to yield an observable current, and the LUMO states become accessible as shown in Fig. 3.1(c). Exploiting this idea we can access both HOMO and LUMO states simply upon changing the bias voltage by using STM tip as an electrode for charge injection. We have also made use of the capability of STM to change tip-sample separation controllably thereby varying the amount of charge being injected into the sample. This enables us to observe new nano-scale phenomenon near the probe-tip as described in the next sections.

A limited number of tunneling studies on organic semiconductors and molecules have been reported previously. Kim *et al.* in 1996 used a thin insulating layer as

tunneling barrier for efficient electron injection process into the sample.<sup>1</sup> However as explained earlier, in our experiments, interface effects from deposition of an insulating layer are eliminated in STM measurements since the thin insulator layer is replaced with a vacuum barrier between the tip and the sample. Similar STM studies as ours have been reported by Datta *et al.*<sup>2</sup> on self-assembled monolayers where a total voltage drop occurs between the tip and the sample and more recently by Ruppel *et al.*<sup>3</sup> on a Pn diode where they observed variation I-V characteristics of Pn films with varying thickness of the films. However they did not perform any spectroscopic measurements by varying tip-sample separation thereby injecting different amount of charge carriers in the film. Other works in the literature include STM study by Alvarado *et al.*<sup>4,5</sup> and Kemerink *et al.*<sup>6,7</sup> on another semiconducting molecule CuPc. That work did investigate the variation of tunnel current with voltage and tip-sample separation, although those experiments relied on the tip and sample making physical contact and thus eliminating the vacuum barrier.

## **3.2 Experimental**

Pentacene thin films were deposited in UHV conditions using a sublimation method. The substrate used was oxidized SiC which is a wide band gap semiconductor. The tunnel current spreads into the Pn film and provides us with a way to measure charge transport through these highly ordered molecular films. In the following sub-sections UHV deposition of Pn molecules and SiC substrate preparation by H-etching is described in detail, along with results from AFM and STM imaging of these thin films.

### **3.2.1 UHV deposition of Pn molecules**

Pentacene molecules used in our experiments were bought from Aldrich. The Pn was deposited by sublimation from a pyrolytic boron nitride crucible under UHV conditions. The base pressure of our preparation chamber is less than  $5 \times 10^{-10}$  Torr. The crucible is capped with a perforated tantalum foil where the hole in the foil acts as a point source of Pn molecules. The crucible is wrapped with a tungsten filament for controlled heating. A type-K thermocouple is used to monitor temperature of the crucible near the tantalum foil cap. The source/crucible temperature is typically kept at 210°C for Pn sublimation. In order to ensure the cleanliness of the deposited film the source was degassed at about

120°C for about 12 hrs prior to deposition in order to get rid of low vapor pressure contaminants. During deposition process a typical pressure recorded in the ion gauge was around  $5 \times 10^{-8}$  Torr. Often to ensure further cleanliness of the whole process, a mock deposition step was performed prior to actual deposition to get rid of top layers of Pn molecules from the crucible. Deposition was monitored using a quartz crystal thickness monitor with a deposition rate of roughly 1 nm per minute. The substrate was kept at room temperature during deposition process. As presented below in Section 3.3, we were able to obtain 8-10 ML of Pn regularly in a typical deposition process with large domains of Pn showing a dendritic growth pattern, as observed by prior workers and indicative of high quality film growth.<sup>8</sup>

### **3.2.2 SiC substrate preparation**

SiC, which is a wide band gap semiconductor, was chosen for use as the substrate material for the Pn thin film growth since its large band gap prevents transmission of the current into the SiC itself. Several poly-types of SiC exist. For our work we have used one of the most common, 6H-SiC, with the surface being (0001) oriented with nominally no miscut. The wafers were n-type doped having a doping density of about  $10^{18}$  cm<sup>-3</sup>. By etching the as-received wafer with hydrogen, atomically flat SiC surface were prepared as described below.

The as-received wafers contain many scratches which arise from the polishing process and the surface is not suitable for thin film growth. In order to remove these scratches from the wafers, hydrogen etching is used.<sup>9</sup> We use a tantalum strip heater on which the SiC sample is mounted. By resistively heating such a foil to about 1650°C under a hydrogen environment we get atomically flat surfaces without any scratches, as seen from AFM images. The H-etching is performed using pure H<sub>2</sub> gas, at 1 atm pressure and with a flow rate of about 10 lpm. H<sub>2</sub> gas upon contact with the hot Ta foil dissociates into H atoms and reacts with SiC to produce the etching process. Figure 3.2 shows SiC surface before and after H-etching. After H-etching large atomically flat terraces with uniformly spaced steps are present on the surface, with the steps arising from unintentional miscut of the wafer. A typical terrace width is ~20 nm, which is large enough for STM experiments.

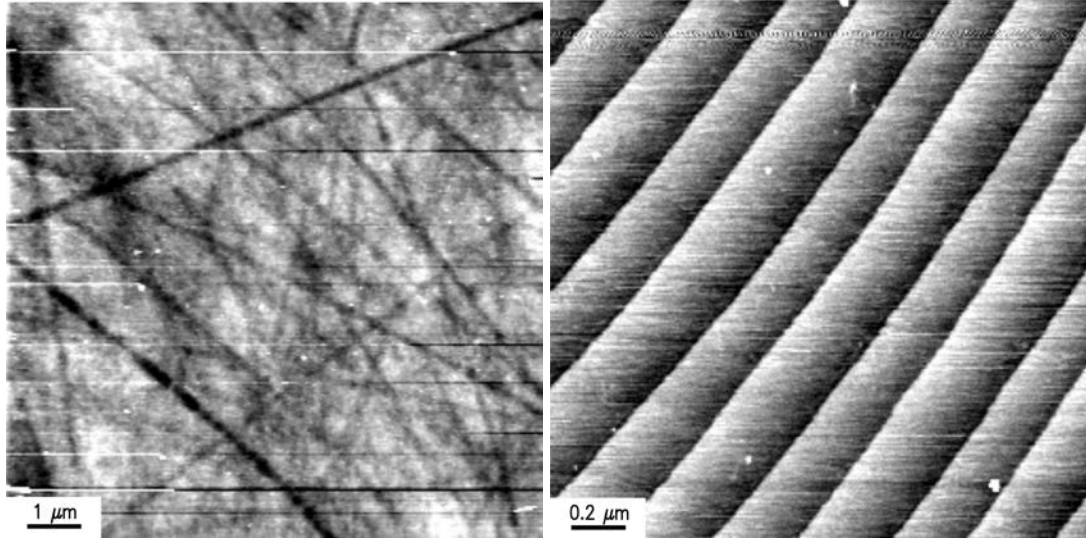


FIGURE 3.2: Comparison of as received SiC sample (left) with sample after H-etching (right). Images were acquired with contact mode AFM.

Following H-etching, the samples were cleaned using solvents and introduced into UHV. They were then thoroughly degassed at about 600°C for more than 2 hrs to eliminate any molecules adsorbed onto the surface during the sample transfer process from the H-etching chamber to the STM chamber through air. The substrates were then oxidized by leaking 99.995% pure molecular oxygen into the UHV chamber through a leak valve. The substrate temperature was held at 600°C during the oxidation process, and the substrate is exposed to ~5000 Langmuir of oxygen. This oxidation process is known to produce 1-2 ML of oxide on top of the SiC substrate, as verified by Auger electron spectroscopy. The oxide layers thus formed help in forming large domains of Pn as is typically observed in case of oxidized Si surfaces explained earlier in Chapter 1. The sample is then transferred *in situ* to the STM/STS chamber for further analysis.

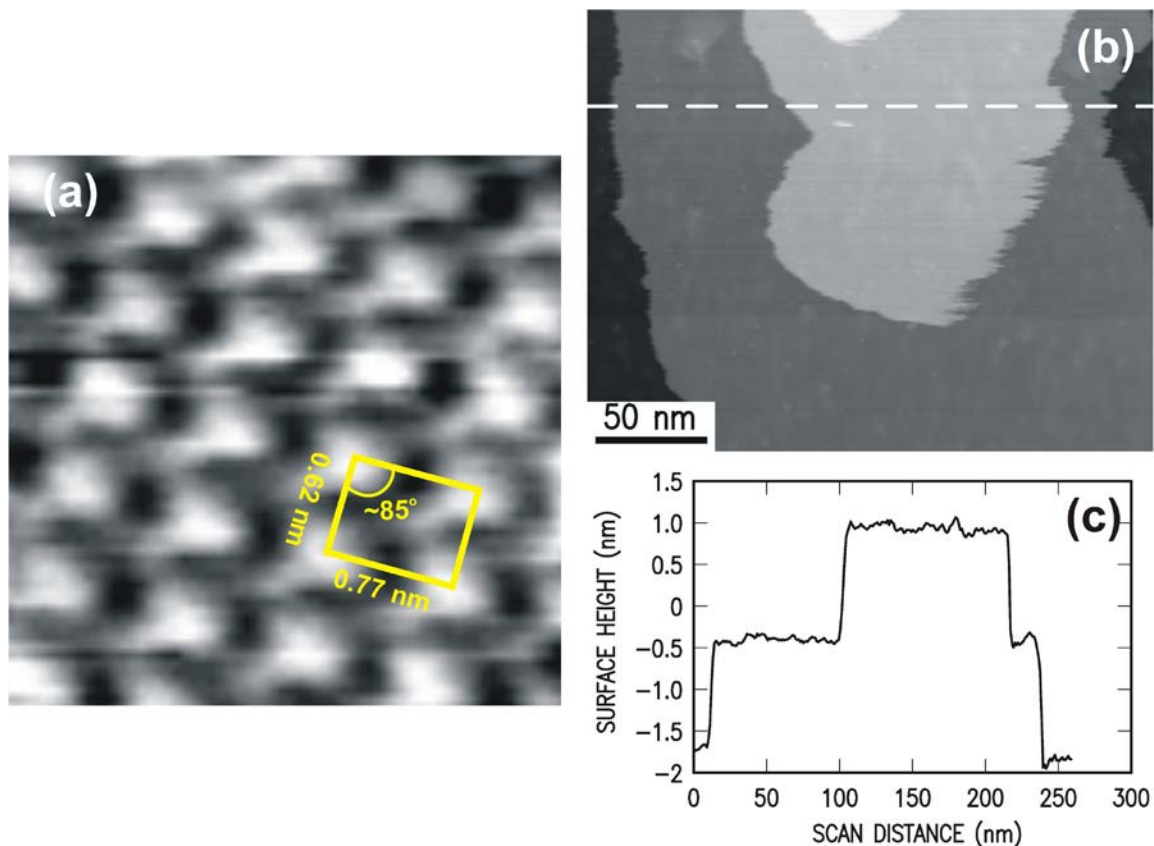


FIGURE 3.3: (a) High resolution STM image of Pn thin film. Each protrusion represents a Pn molecule. The image was taken at  $-2.7$  V sample voltage. A surface unit cell is marked by yellow lines. (b) Large-scale STM image of layer-by-layer growth pattern of Pn film. Image was acquired at  $-3.0$  V. (c) A line scan of image in (b), taken along the dashed line in the image.

### 3.3 Results from STM and AFM imaging of Pn

STM images were acquired in a constant current mode, using a constant current value of  $0.1$  nA unless otherwise specified and with sample-tip voltages specified below. Figure 3.3(a) shows a high resolution STM image of the Pn film, with a unit cell is marked on the surface. Each lobe shows a single molecule. In the image the lobes are seen to be slightly elongated, resembling shape of a light bulb. This shape arises because the inequivalent Pn molecule at the center of the molecule is about  $0.3$  nm below the other 4 molecules, which are at the four corners of the unit cell. As shown in Fig. 1.5(b) the two types of inequivalent molecules make an angle of  $\sim 53^\circ$  with respect to each other, hence giving rise to the “light bulb” shape. From the larger STM image of Fig. 3.3(b) it is

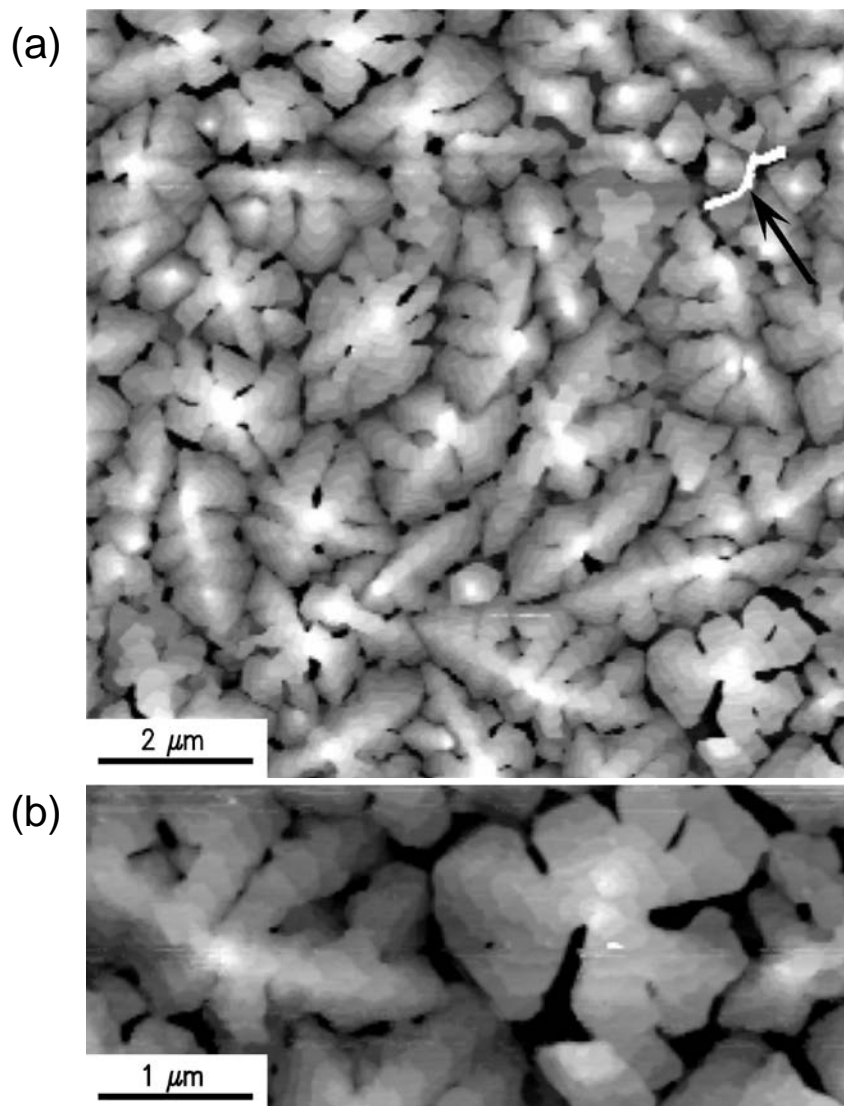


FIGURE 3.4: (a) Large image of Pn film acquired using tapping mode AFM. The bright region indicated by an arrow reveals segregation of Pn molecules. (b) Multiple terraces are clearly visible in the close-up image.

clearly observed that the Pn thin films growth in a layer-by-layer mode. In order to confirm the thin film structure in which the Pn molecules are expected to stand up with their long molecular axis almost perpendicular to the substrate, we took a line scan from the image and the result is shown in Fig. 3.3(c). The height of each layer is close to 1.5 nm which confirms the fact that the molecules do indeed align with their long axis almost perpendicular to the substrate surface. In order to characterize the large scale structure of the films, AFM images were acquired (using tapping mode as is normally used for

imaging soft organic molecules). These AFM images are acquired in air, after completing STM/STS studies in the UHV chamber. Figure 3.4 shows AFM images in which the dendritic growth pattern of Pn film is clearly observed. Large ordered domains of Pn are obtained, which are suitable for STM studies. These AFM images are usually acquired a few days after deposition and subsequent STM/STS measurements. Often times Pn molecules segregate during that time period, and show up in AFM images as bright spots. One such segregated region is marked by an arrow in Fig. 3.4(a).

### 3.4 Results from tunneling spectroscopy

Local electronic properties of Pn film can be obtained using STS techniques. Normalized conductance measurements yield information about the LDOS. Another important advantage of STM is that the tip-sample separation can be varied and different amount of charge can be injected into the sample. A new method for data acquisition was used for controllable variation of tip-sample separation. Effect of transport properties of organic film on tunneling current was studied using these methods.

#### 3.4.1 Normalized conductance measurements

Normalized conductance measurements  $(dI/dV)/(\overline{I/V})$  were performed and a typical spectrum is shown in Fig. 3.5. Many such spectra are regularly acquired on different samples using different probe tips. Although a slight variation in the shape of these spectra is sometimes seen, the basic features are very reproducibly observed. The STS spectra reveal two peaks, as indicated by arrows in Fig. 3.5. The approximate locations of the peaks are at  $-2.25$  and  $0.80$  V, respectively. The apparent width of the band gap is then found to be  $2.1 \pm 0.1$  eV. For comparison, we examine band gap values reported in the literature. From STS on Pn films deposited on Cu(119) a molecular gap opening of  $2.35 \pm 0.05$  eV has been reported.<sup>10</sup> The same value has also been quoted with STS on a monolayer of Pn on Ag/Si(111) substrate.<sup>11</sup> For thin films, gap values ranging from 1.97 to 2.68 eV have been obtained with optical measurements.<sup>12,13,14</sup> Moreover, the electronic properties of solid Pn for two different crystalline phases-S (solution phase crystallized) and V (vapor phase crystallized)-were determined using *ab initio* calculations<sup>15</sup> to be 2.2

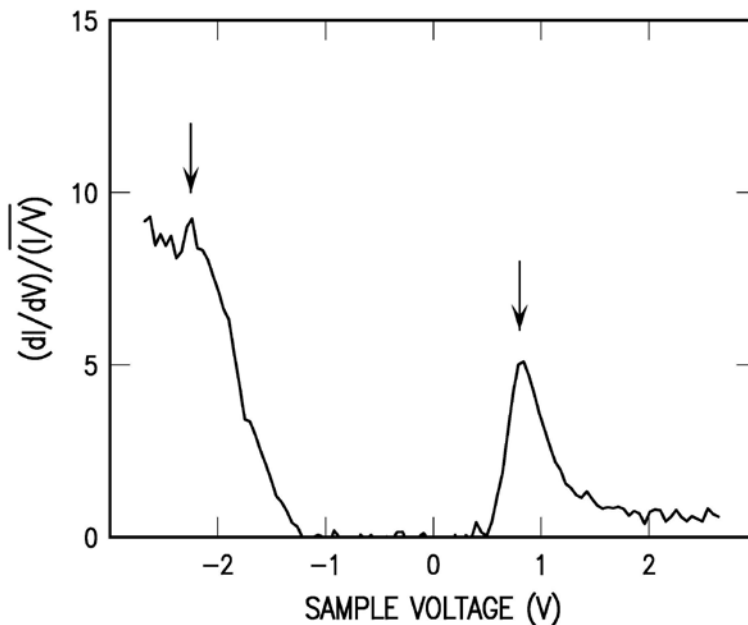


FIGURE 3.5: Normalized conductance spectra from a Pn thin film. HOMO and LUMO levels are indicated by arrows.

and 1.9 eV, respectively. The phase with a higher intermolecular overlap gives rise to a narrower molecular gap (1.9 eV) and larger bandwidth of the HOMO and LUMO. From the above discussion it is apparent that our result for band gap of about 2.1 eV matches well with earlier observations using both experimental and theoretical methods.

Nevertheless, as discussed in the following section, the shape of the STS spectra of Pn can potentially depend on the magnitude of the tunneling current used, because of transport limitations in the current flow. For this reason, we will revisit results obtained from normalized conductance spectrum in the Discussion Section later in this chapter.

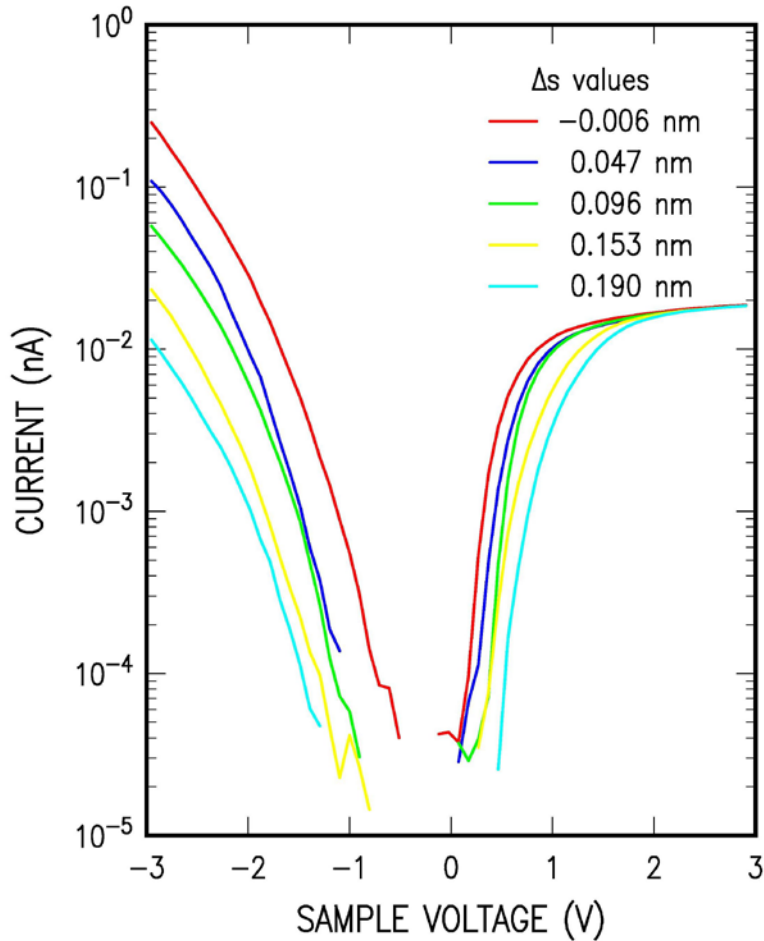


FIGURE 3.6: I-V curves of Pn film acquired with different tip-sample separations.  $\Delta s$  is the relative tip-sample separation, with lower values meaning that the tip is moved closer to the sample surface.

### 3.4.2 Saturation of tunnel current in Pn thin films

In order to extract more information about the sample surface we have performed systematic measurements varying the set point current thereby changing tip-sample separations. The results are shown in Fig. 3.6. In this experiment, I-V curves were acquired at specific tip-sample separations as determined by the constant current value (the so-called *set-point* current) prior to the I-V curve. By changing the set-point current, the relative separation  $\Delta s$  between the tip and the sample is changed. Values for  $\Delta s$  were determined after the I-V measurements by recording the variation of tunnel current with absolute tip-sample separation  $s$ , at a particular sample voltage. Results from such I-s

curves, acquired at  $-3\text{ V}$  and  $-2\text{ V}$  respectively, are shown in Fig 4.7. From these curves we calculated the relative separation  $\Delta s$  between the probe-tip and the sample

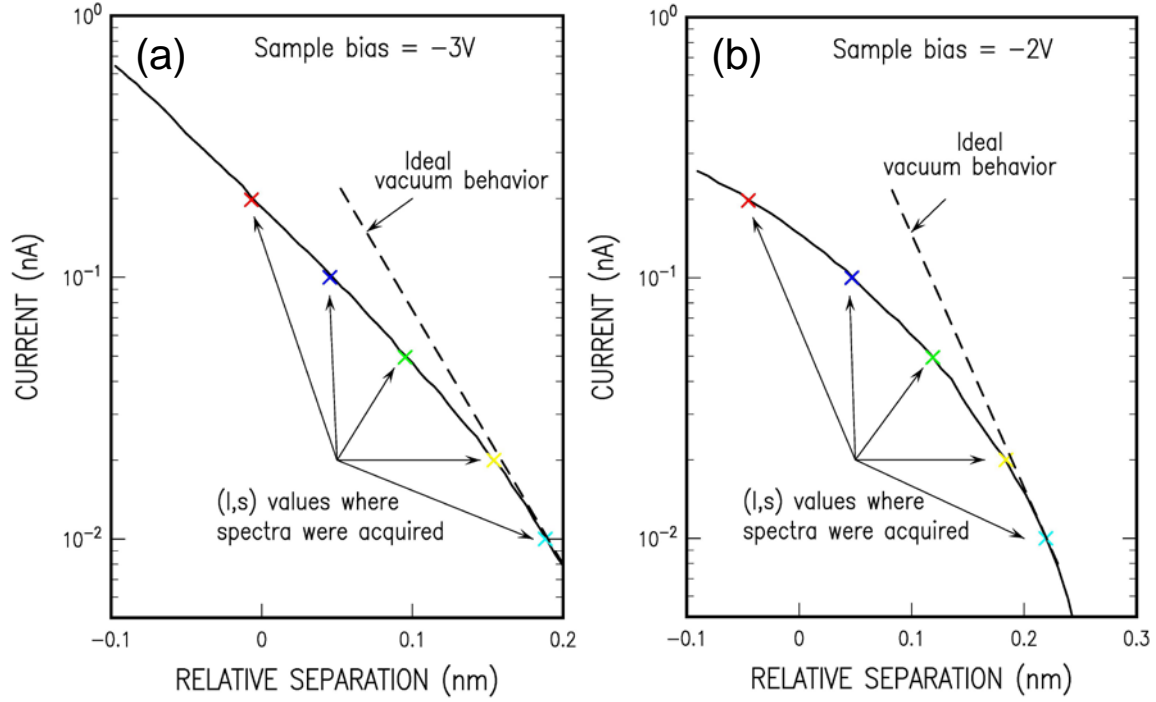


FIGURE 3.7: I-s measurements performed at different sample voltages as compared with ideal vacuum behavior shown with dashed lines. Cross-marks indicate set-point current values for which I-V curves were obtained as shown in Fig. 3.6.

corresponding to the constant currents. These  $\Delta s$  values are shown in Fig. 3.6 and are also indicated with cross-marks on the corresponding I-s curve shown in Fig 3.7.

The most interesting and surprising result obtained from the I-V curves shown in Fig. 3.6 is that the tunnel current strongly saturates at positive sample voltages. This saturation is direct evidence that the flow of the tunnel current is limited by some sort of charge transport mechanism in the sample. Moreover, from Fig. 3.7 it is seen that even for negative sample-tip voltage, there is significant deviation from the ideal vacuum behavior as the tip-sample separation is reduced. The ideal vacuum behavior, shown by dashed lines in Fig. 3.7, corresponds to  $I \propto \exp(-2\kappa s)$  with an “ideal” value (appropriate to metal-vacuum-metal tunneling) for  $\kappa$  of  $10\text{ nm}^{-1}$  used in the figure. From Fig. 3.7 it is observed that, even at negative sample voltages, moving the probe-tip towards the sample does *not* produce an increase in the tunnel current by enough amount expected from ideal

vacuum behavior; the slope of the  $\log(I)$  vs.  $s$  curves for small  $s$  values in Fig. 3.7 are less than half of the ideal curve, implying  $\kappa$  values less than  $5 \text{ nm}^{-1}$ . And, for the large positive voltages shown in Fig. 3.6 the current is completely saturated, implying a  $\kappa$  value of 0. Figures 3.6 and 3.7 thus provide the first evidence that charge transport properties of the sample do have significant effect on tunnel current. It should also be pointed out that using a single measurement technique we are able to see transport limitation in tunnel current for both filled (HOMO) and empty (LUMO) states.

It is important to note that, even in the absence of transport limitations in the semiconductor, tunneling characteristics of semiconductor-vacuum-metal junctions can be somewhat "non-ideal" in the sense that they differ from those of metal-vacuum-metal junctions. As already discussed in Section 2.2, some of the voltage drop across the junction can occur in the semiconductor itself, simply because of the electrostatics (continuity of the normal component of the displacement field across the vacuum-semiconductor interface). Such *tip-induced band bending* tends to produce I-V curve that are shifted to voltages with greater magnitude. This shift does produce associated changes in the  $\kappa$  value, but those changes are generally quite small (<10%) for voltages more than a few tenths of a V away from the band edges. In contrast, the large changes in the  $\kappa$  values seen in Figs. 3.6 and 3.7 imply not only a large voltage drop in the semiconductor, but one which *increases as the current increases*. Hence, we associate it with a transport-induced voltage drop in the semiconductor. This type of effect thus implies a transport limitation for the current that occurs in the semiconductor, rather than the usual situation in tunneling in which the limiting factor is in the transmission across the vacuum barrier itself.

The above measurements demonstrate transport limited tunnel current in Pn films conclusively. But, they suffer from several limitations. First it is not possible from the I-V curve alone to detect the saturation of the current for negative sample voltages. This limitation is because the changes in tip-sample separation are obtained in these measurements by varying the set-point current prior to acquiring each I-V curve. Also, the entire time scale over which the measurements are performed (in which the set-point current is progressively changed) is quite long, several minutes at least. During acquisition of such a set of I-V curves the probe-tip might drift away from the point of

interest due to thermal effects. Also the electronic structure of the tip might change with time, which makes the measurements process quite difficult to perform. Hence a faster and more reliable data acquisition was developed, as described below.

### **3.4.3 Spectroscopy with discrete $\Delta s$ (tip-sample separation)**

In this method we directly and systematically move the probe-tip closer to the sample surface, thereby injecting more charge carriers into the sample. For each I-V curve the STM feedback loop is opened, and current is measured by sweeping the voltage in the appropriate range. Then the probe-tip is automatically moved by a specified amount towards the sample typically (0.05 nm), and another I-V curve is obtained. One can continue this process till the point where the sample surface begins to show damage. Once the appropriate range of  $\Delta s$  has been determined such that we can inject current without changing electronic properties of the sample surface, sets of spectra can be acquired easily and quickly. Additionally, images are acquired periodically to check the quality of the surface after each set of spectra. Figure 3.8 shows a set of spectra acquired using the method described above.

In Fig. 3.8 we again see saturation of the tunnel current at large positive sample voltages. These measurements, however, extend over a large range of  $\Delta s$  values than those of Figs. 3.6 and 3.7, and a new feature appears in the data. When we move the probe-tip towards by more than 0.25 nm the current suddenly increases, and by moving it a little further by 0.05 nm it starts to decrease again. Those I-V curves are circled in the image. Usually this behavior is accompanied by a slight damage to the surface and we see a small dip in the accompanying STM images at the point where spectra were acquired. Observation of damage to the surface probably means that the vacuum barrier completely collapses and the probe-tip just starts touching the surface or forms a conducting bridge between the tip and the sample surface which results in a large increase in the tunneling current. In this process the surface gets damaged and most likely the electronic as well as structural properties of the surface alter significantly. In this case, if the tip is moved even further the current is seen to decrease. In our analysis below we avoid this damaged threshold in the portions of the data that we analyze.

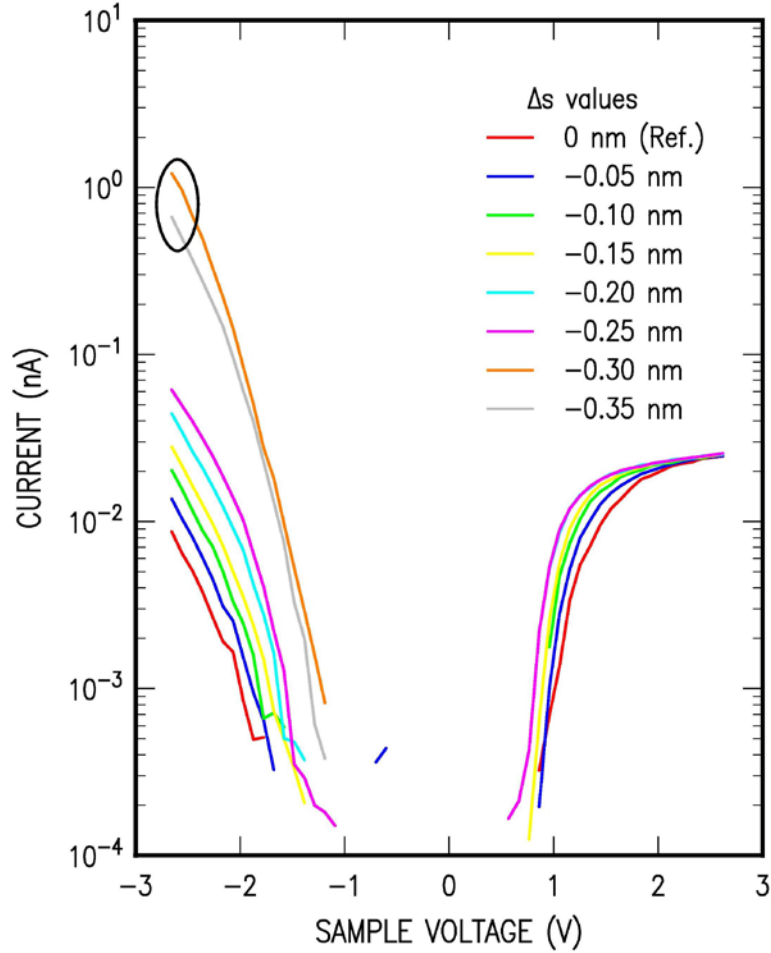


FIGURE 3.8: I-V curves obtained from a Pn thin film, by systematic  $\Delta s$  variation. Starting from red curve in the bottom, the probe-tip was consecutively moved by 0.05 nm to inject more current starting, from 10 pA (red) to about 1 nA (orange).

From the data of Fig. 3.8 we can deduce  $\kappa$  values as a function of voltage. Defining the  $\kappa$  value as that which gives a dependence of the current on separation of  $I \propto \exp(-\kappa s)$ , then we have  $\kappa = -0.5 d \ln I / ds$ . From the neighboring I-V curves we compute  $-0.5 \Delta \ln I / \Delta s$ , and results are plotted in Fig. 3.9 for both negative (blue) and positive (red) sample voltages using two different probe tips. For positive sample voltage the tunnel current saturates and indeed  $\kappa$  rapidly decays to zero as seen from Fig. 3.9. For negative sample voltage, although there is some variation in  $\kappa$  values, it does not completely collapse to zero. These larger  $\kappa$  values are an indication that there is less transport limitation in tunnel current associated with the HOMO than the LUMO.

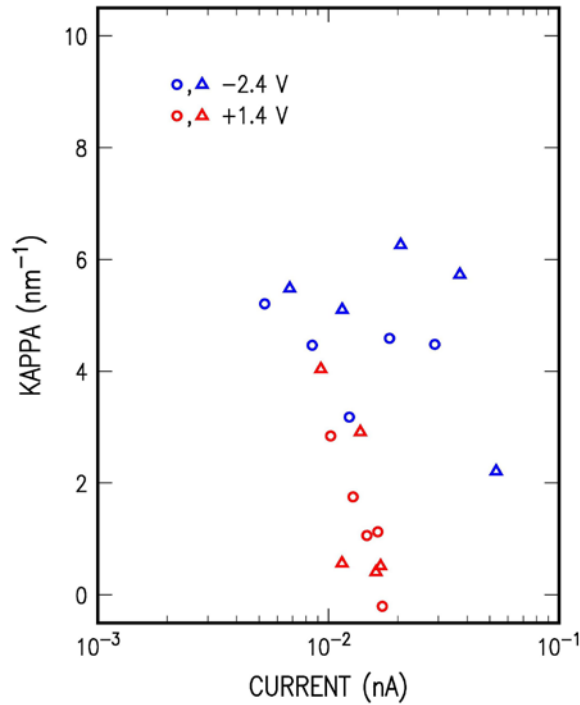


FIGURE 3.9: Calculated  $\kappa$  values for negative ( $-2.4$  V: blue) and positive ( $1.4$  V: red) sample voltages plotted with magnitude of tunnel current. Results shown using triangle and circles are for two different probe-tips.

### 3.5 Discussion

In STS studies of semiconductors, transport of charge carriers within the semiconductors is not well understood. In most cases it is assumed that transport plays no significant role. This is because the resistance of the tunnel junction is about  $1 \text{ G}\Omega$  which is many orders of magnitude higher than the resistance in the sample. A few prior studies have found evidence of transport limited tunnel current for some semiconducting surfaces. Low temperature STM studies on  $\text{Si}(001) 2 \times 1$ <sup>16,17</sup> and H-covered  $\text{Ge}(111)c(2 \times 8)$ <sup>18</sup> surfaces by Takanayagi *et al.* and Dujardin *et al.* lead to the suggestion that the transport of carriers in the semiconductor may be in some way affects the results.<sup>16,18,19</sup> Earlier, Ramachandran *et al.* had observed such effects on  $\text{SiC}(0001) \sqrt{3} \times \sqrt{3} - R30^\circ$  surfaces using room temperature STS measurements.<sup>20</sup> Low temperature work on  $\text{Ge}(111)c(2 \times 8)$  surface by Feenstra *et al.*, following the work of Dujardin, showed evidence of transport limited

current in the semiconductor and clarified the mechanism for this limitation as being associated with charging of midgap states arising from defects in the surface structure.<sup>21</sup> However, none of the above studies show nearly as much evidence of transport limitations as with our results for Pn, in which the tunneling current is completely saturated. Very recently, Berthe *et al.*<sup>22</sup> presented results on current saturation in STS measurements for a single Si dangling bond on a B-doped Si(111) surface. At the end of this Section we analyze our results in a manner similar to that developed by those authors.

To introduce our discussion of transport limitations in the semiconductor current flow, Fig. 3.10 illustrates some aspects of the problem. The probe tip injects current into the film. Some variation in the electrostatic potential will occur across the vacuum gap [voltage drop  $V_1$  in Fig. 3.10(b)] as well as within the semiconductor [Fig. 3.9(c)]. For the situation of interest the Pn films are undoped. In a 3-dimensional model, the electric-field due to the probe tip will fall off radially along the semiconductor surface due to the sharpness of the probe tip. In the absence of any current flow, the electrostatic boundary condition across the semiconductor-vacuum interface will produce a variation in potential along the surface of the semiconductor qualitatively similar to that shown in Fig. 3.10(c).

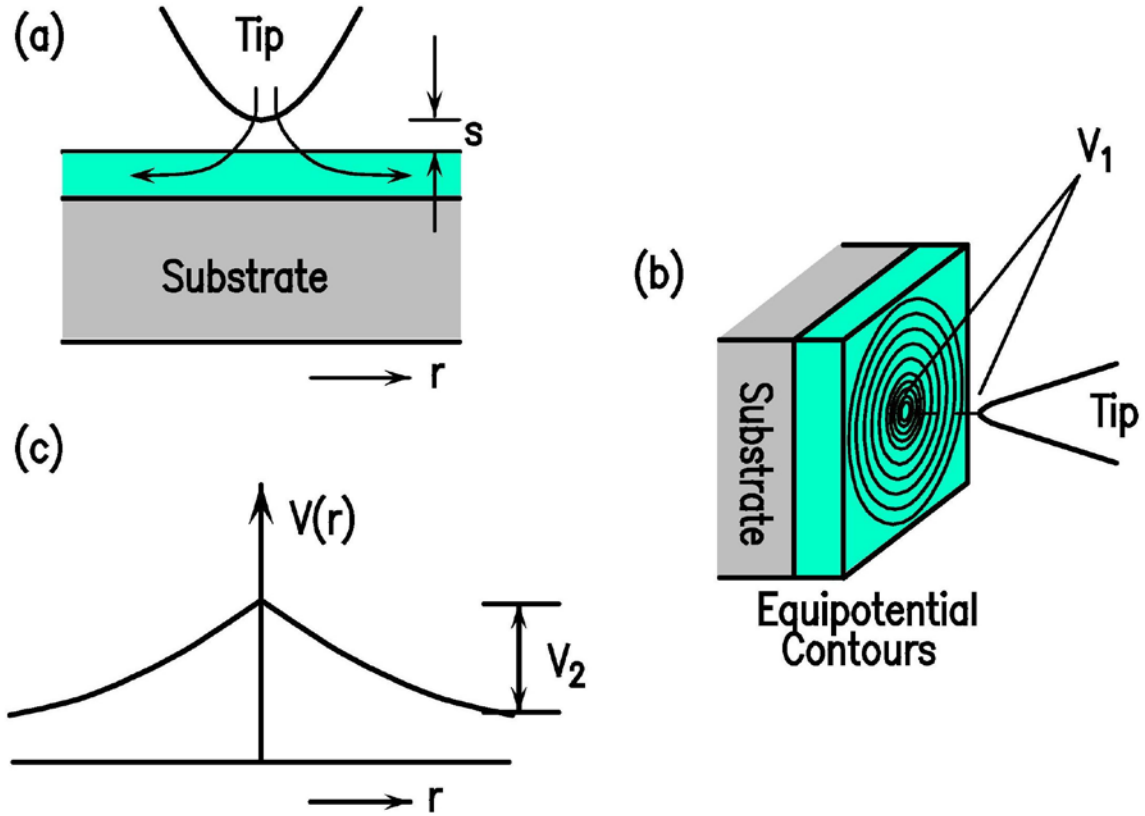


FIGURE 3.10: (a) Current injection from a STM tip and carrier confinement in a Pn film. (b) Constant potential contours (with potential rising towards the center) on Pn surface in the vicinity of probe-tip. (c) Schematic variation of band edge energy.  $V_1$  and  $V_2$  are the voltage drops in the vacuum and the sample respectively.

### 3.5.1 Simple resistance model

As a first step to understand saturation of the tunnel current in the sample, we treat the sample as highly resistive which simply limits the current flow. The model assumes that the tunnel current is proportional to the applied bias voltage according to the relation,

$$I = \frac{V}{R_t}, \quad (3.1)$$

where,  $R_t$  is the resistance of the tunnel junction and depends exponentially on the tip sample separation  $s$  as,

$$R_t = R_t^0 \exp(2\kappa s) \quad (3.2)$$

Under an applied sample voltage, if the voltage drop in the sample is  $\Delta V$ , the decay constant  $\kappa$  takes the form,

$$\kappa = \sqrt{\frac{2m}{\hbar^2} \left( \bar{\phi} + \frac{e\Delta V}{2} \right)} \quad (3.3)$$

We further assume that the voltage drop in the sample  $\Delta V$  is related to the tunnel current and sample resistance  $R_S$  by  $\Delta V = IR_S$ . Using the relation  $I \propto \exp(-2\kappa s)$  and Eqs. (3.1), (3.2) and, (3.3) we get,

$$I = \frac{V}{R_t^0} \exp \left\{ -2s \sqrt{\frac{2m}{\hbar^2} \left( \bar{\phi} + \frac{e}{2} R_S I \right)} \right\} \quad (3.4)$$

We solve this equation for tunnel current  $I(s)$ , and then compute the decay constant  $\kappa$  by the derivative  $\kappa = -0.5 d \ln I / ds$ . Figure 3.11 shows the results from the computation. The parameters used in the computation are  $|V| = 3.0 \text{ V}$ ,  $R_t^0 = 10^7 \Omega$ ,  $\bar{\phi} = 3 \text{ eV}$ , and the values of  $R_S$  ranging from  $10^8$  (red curve) to  $10^{12} \Omega$  (cyan curve). Data points shown by triangles are for comparison.

It is clear from Fig. 3.11 that this simple model with constant sample resistance is insufficient and does not fully agree with the experimental spectroscopic results. The variation in the computed decay constant  $\kappa$  is much more abrupt than the variation of  $\kappa$  found in the experiments. Hence this model is inappropriate to completely explain the observed saturation of tunnel current in the Pn thin films, and additional physical effects must be considered. In the next sub-section we present a more detailed discussion of the electronic effects in the sample that occur in the vicinity of the probe-tip.

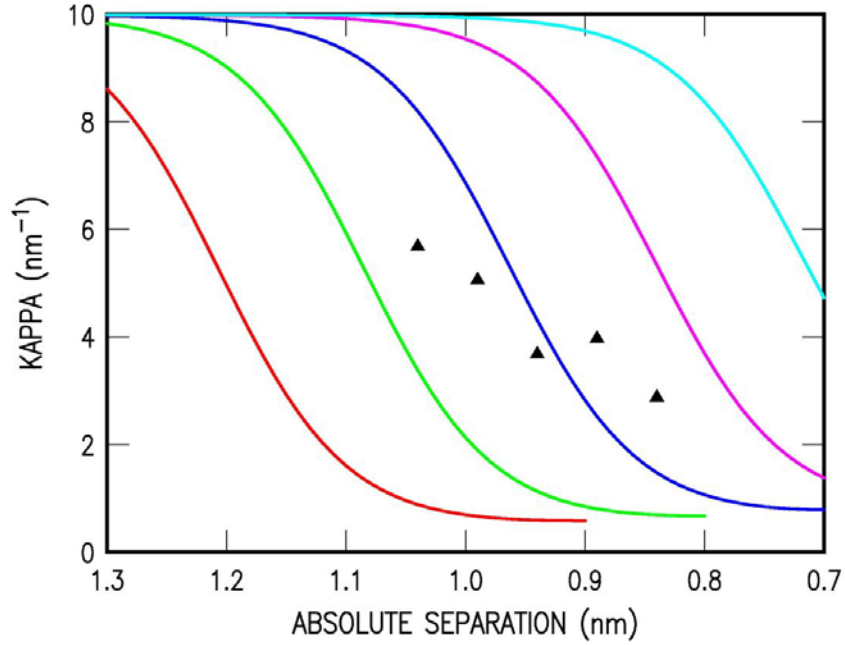


FIGURE 3.11: Computed curves with different sample resistances  $R_S$  ( $10^8 \Omega$  shown in red to  $10^{12} \Omega$  shown in cyan) are plotted by solid lines. Points shown with triangles are from experiments. These points are positioned on the x-axis to match the theoretical curves.

### 3.5.2 Space charge limited tunnel current

Now, to account for the transport of carriers in the undoped Pn films, we must treat them as insulators so that the carrier concentration will vary as a function of distance from the tip. The injected carriers move out into the sample from the region directly under the probe-tip. Considering the narrow HOMO and LUMO bands this transport process can be quite slow relative to the tunneling rate through the vacuum barrier. As a result there can be a charge buildup in the sample near the probe-tip. Hence the voltage drop in the sample increases and there is more band-bending in the sample with a corresponding decrease in voltage drop through the vacuum junction. This band-bending restricts more charges to be injected from the tip even if it is pushed closer to the sample surface which results in saturation of tunnel current. This situation is analogous to space charge limited current (SCLC) observed for the case of charge injection into insulators through metal electrodes making ohmic contact with the sample.<sup>23,24</sup>

For organic semiconductors SCLC has been observed previously.<sup>12</sup> In a typical SCLC regime in a 1-dimensional geometry and with an electrode in intimate contact with the semiconductor a simple relationship  $I \propto V^2$  exists between current and voltage. The field varies as  $x^{1/2}$  where  $x$  is the distance from the electrode, and the carrier density varies as  $x^{-1/2}$ . However in the case of charge injection by STM tip the physical situation is quite different. Charge is injected from the tip, and hence is mostly confined in the vicinity of the probe-tip in the nano-scale regime, and furthermore the voltage drop is split between the vacuum and the semiconductor. As a consequence, a simple relationship of  $I \propto V^2$  which is observed under typical SCLC case is not appropriate in our experiments. A full description of the SCLC in our geometry is involves a coupled solution of Poisson's equation and the current transport equation, in 3-dimensions, something that we have not yet achieved. Nonetheless we can estimate the number of charge carriers by few simple assumptions. Current density  $j$  is related to the number of charge carriers  $n$ , mobility  $\mu$  and electric field  $E$  as,

$$j = ne\mu E. \quad (3.5)$$

We assume a carrier mobility of our Pn films to be of the order of about  $1 \text{ cm}^2\text{V}^{-1}\text{s}^{-1}$  (as seen in prior experiment<sup>25,26,27,28</sup>) and assume a linear relationship to exist between mobility and electric field. In STM the electric field in the sample due to the probe-tip extends across the sample radially by tens of nanometers (of the order of the probe-tip radius of curvature). Hence, for a voltage drop in the semiconductor of 1V the field will be less than 0.1 V/nm, and for a current density of  $1 \text{ nA/nm}^2$  we estimate a carrier density of  $\sim 10^{18} \text{ cm}^{-3}$ . If we compare this value with what occurs, at low current values, in doped semiconductors in which the doping density varies from  $10^{18} \text{ cm}^{-3}$  to much lower values, then we know that the band bending in the semiconductor does indeed significantly change over this range of charge densities. (It is important to note that, e.g. for n-type material and positive sample voltages, the space charge in the doped case is positive, whereas the electron density in the SCLC case is negative, so the situations are not exactly analogous). Thus, a carrier density this large suggests that we can get into the regime where transport limitation starts to have significant effect on tunneling current.

We can use an additional argument to extract the rate of hopping rate for carriers in the LUMO band for the situation where we see a clear saturation of the tunnel current.

The argument is similar to that given by de la Broïse *et al.*<sup>29</sup> and Berthe *et al.*<sup>30</sup> for the case of tunneling current through a single Si-dangling bond on a Si(111) surface. Let us define  $W_t$  as probability per unit time for the tunneling of an electron between the tip and a LUMO state localized on a molecule opposite the tip. We are regarding the LUMO band to be formed by the overlap of such states on neighboring molecules, with hopping occurring between neighboring states (it is important to note that the known width of the LUMO band, 0.1 eV, is indeed quite narrow). We further denote by  $f$  the probability that the particular state is occupied. Then the expression for tunnel current can be written as

$$I = -e(1 - f)W_t, \quad (3.6)$$

which simply expresses the fact that the electron tunneling is possible only when the state is empty. In the steady state regime the tunnel current must be equal to

$$I = -efW_{hopp}, \quad (3.7)$$

where  $W_{hopp}$  is the probability per unit time for the emission process which is a hopping rate between the states localized on the molecules. Eliminating  $f$  between Eqs. (3.6) and (3.7) we obtain

$$I = e \frac{W_t W_{hopp}}{W_t + W_{hopp}}. \quad (3.8)$$

When rate of tunneling is much higher than the emission process i.e.,  $W_t \gg W_{hopp}$  then we get the condition for space charge limited current and  $I = I_{sat}$ . Using this condition, Eq. (3.8) is modified as,

$$I_{sat} = eW_{hopp}. \quad (3.9)$$

Using  $I_{sat} = 25$  pA from Eq. (3.9) we get a hopping rate of  $1.6 \times 10^8$  s<sup>-1</sup>.

Physically this hopping rate would determine charge transport at least in the vicinity of the probe-tip. The time scale is of the order of  $10^{-8}$  s which is indicative of strong polarization of the molecule<sup>31</sup> when it gets charged by an electron tunneling into it. As discussed by prior author,<sup>31</sup> a molecular ion is formed which in turn induces a lattice deformation and consequently there is a self-trapping type of effect in which the charge is strongly localized. This strong localization of charge leads to relatively low hopping rates, thus producing the space charge type of effect in the tunnel current.

The experimental method developed above for Pn can be used to look for evidence of transport limited tunnel current in other systems. We have performed similar measurements on SiC(0001) surfaces with different reconstructions. In particular we have focused on Si-rich SiC(0001)  $\sqrt{3} \times \sqrt{3} -R30^\circ$  and  $3 \times 3$  reconstructed surfaces both of which are Mott-Hubbard insulators. Measurements on a graphene surface (C-rich surface of SiC) are also performed and a comparative study of all surfaces is presented in Chapter 4. In the next sub-section we return to re-examine the normalized conductance spectra of Pn (as already presented in Fig. 3.5), to see if the effects of transport/space charge limited tunnel current modify our conclusions of that data.

### **3.6 Effect of transport limitation on STS spectra**

With observation of transport/space charge limited tunnel current we need to revisit the results obtained from the normalized conductance spectra. It is seen from the normalized conductance spectra shown in Fig. 3.5 that the so called LUMO level shows a sharp peak like feature. However if the tunnel current has limited transport in the semiconductor, then the current tends to saturate and thus they might affect the shape of this spectral feature. In particular, if less current is injected into the semiconductor during the measurement, then the peak should shift towards higher positive sample voltages. This is indeed what we obtain by injecting different amount of charge into the semiconductor by systematically varying the tip-sample separation. The results are shown in Fig. 3.12 are obtained by taking numerical derivative of some of the spectra shown in Fig. 3.8. The spectrum at the top was taken at a set point current of 10 pA. The next two spectra were taken by progressively pushing the probe-tip by about 0.1 nm each towards the sample (corresponds to set points of about 28 and 50 pA respectively). The spectrum at the bottom is the same spectrum as Fig. 3.5 taken at nominal set point current of 0.1 nA. With increase in injected current the LUMO peak shifts as indicated by arrows. The shift is roughly 280 meV which is another, albeit indirect, signature of current being limited by electron transport in the sample.

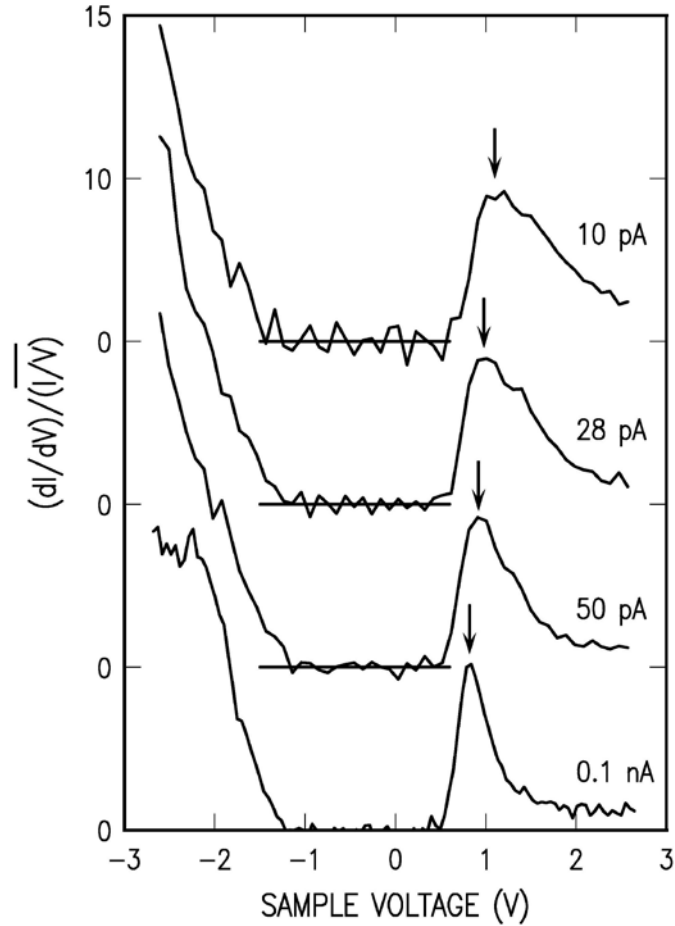


FIGURE 3.12: Series of tunneling spectra with varying tip-sample separation. Consecutive spectra are shifted upwards for clarity. The zero levels for  $(dI/dV)/(I/V)$  are indicated by horizontal lines. Set point currents are indicated for each spectrum.

### 3.7 Effect of oxygen on tunneling spectra

A disadvantage of using Pn in organic electronics is the susceptibility of the Pn molecules to degradation by several means, including oxygen, hydrogen and water impurities. In this section we describe effect of impurities on tunneling spectra for Pn thin film samples. In particular the effect of oxygen will be discussed.

We regularly use pure dry molecular oxygen for oxidation of the SiC substrates in our preparation chamber. Typically oxygen is introduced by a leak valve at a partial pressure of  $1 \times 10^{-5}$  Torr for 30 min to an hour for oxidation of the SiC. If we then immediately start the Pn deposition process, we find that the STS results show

significantly different results as compared to the normalized conductance spectra described earlier.

Figure 3.13 shows various STS results from Pn, comparing spectra on the “degraded” (exposed to oxygen during deposition) Pn with conductance spectrum for “non-degraded” or usual Pn. The dashed lines indicate spectra on non-degraded Pn and solid lines are acquired for the degraded Pn case. Two distinct effects are seen which are shown in Fig. 3.13(a) and (b). A clear tailing of the band edge for valence band is observed in case of Fig. 3.13(a). Figure 3.13(b) shows another spectrum which shows considerable narrowing of the band gap compared with a normal spectrum. Since most of the narrowing is in the valence band side, means more acceptor like character for these degraded Pn films. Hence oxygen acts as a p-type dopant for Pn. It should be made clear that these spectra were acquired on different samples using different probe tips. We almost always obtain tunneling spectra which can be broadly classified into two different categories as shown in Fig. 3.13(a) and (b). In one case, tailing of the valence band edge into the band gap is obtained as shown in Fig. 3.13(a). In the second case the band gap narrows considerably than that of pristine Pn films which is shown in Fig. 3.13(b).

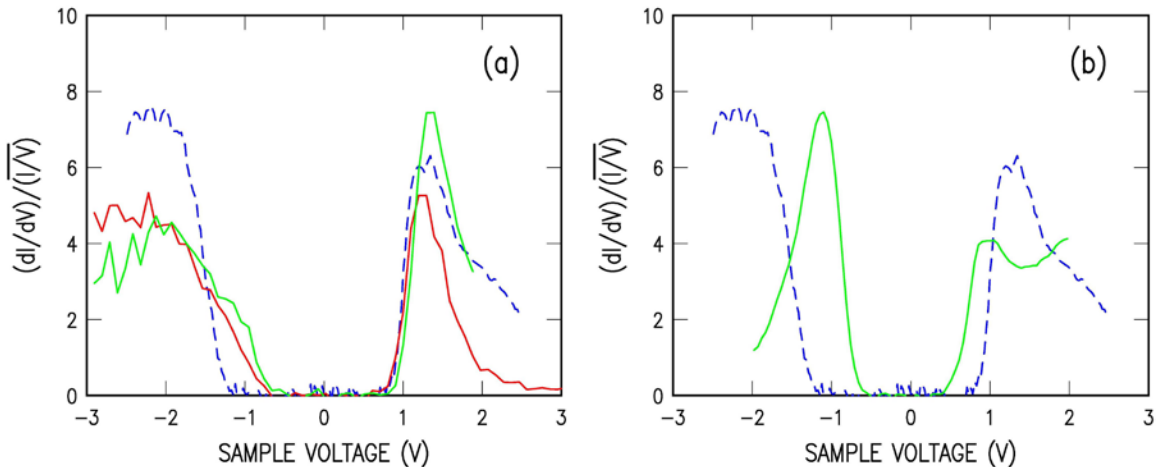


FIGURE 3.13: STS spectrum of Pn films. Solid lines are spectra from "degraded" Pn films, illustrating (a) tailing of valence band edge, and (b) narrowing of band gap. Solid For comparison, the dashed line in both (a) and (b) show a spectrum from a pristine Pn films.

In order to understand the variation in spectra, we have to know if oxygen reacts with Pn to create complex species or simply gets trapped in the film and retains its

molecular form. We can rule out the later case as it is known that in vacuum, oxygen molecules simply diffuses out of the Pn film without leaving behind electrically active electronic states that would lead to a doping of the film.<sup>32</sup> In order to check the effect of oxygen we prepared thin films in an oxygen free environment in UHV. Then we exposed the sample to several Langmuirs of molecular oxygen. STS observation in those samples (not shown here) does not show any change in conductance spectra due to the oxygen exposure. Since those spectra remains unchanged we can safely conclude that in our case the surface of Pn film does not simply react with molecular oxygen (it can react with *atomic* oxygen, but that was not used in our experiment). Our conclusion is supported by observations of Vollmer *et al.*<sup>32</sup> where ultraviolet photoelectron spectroscopy (UPS) was used for surface characterization of Pn films. Hence we conclude that *during deposition* (i.e. in the gas phase, or due to the enhanced energy of the hot molecules that are being deposited) oxygen probably forms some sort of complex species of Pn and gets incorporated into the film and it does not prefer to stay in molecular form. The differences between spectra shown in Fig. 3.13(a) and (b) are further explained below.

This presence of oxygen in the film is expected to alter the properties of the film as observed in the STS experiments. This is because the pristine  $\pi - \pi^*$  bonds gets disrupted by the formation of C – O bonds. These types of chemical defects are known to produce gap states in Pn band gap shown by theoretical calculations<sup>33,34</sup> as well as recent experiments<sup>35,36</sup> and is known to affect electronic transport properties.<sup>37,38</sup> For a simple case in which oxygen forms a bridge between neighboring Pn molecules is known to produce gap states located at about 0.33–0.4 eV above the valence band edge. However more complex configurations contribute to shallower states in the gap. Hence our observation of amorphous like band tails can be explained by the fact that the oxygen indeed produces some complex species in the film to create shallow states near the valence band leading to band tailing. We also observe considerable band gap narrowing for these “degraded” Pn films as shown in Fig. 3.13(b). This narrowing of the band gap can also be explained from the above arguments. The onset of HOMO and LUMO states occur at lower voltages because of the gap states introduced in the sample by oxygen. Hence we conclude that oxygen does play an important role in Pn films even under UHV conditions by doping the sample thereby creating acceptor states and also localized states

are formed closer to the valence band edge giving rise to band tailing and band gap narrowing.

### 3.8 Summary

To summarize work done on Pn thin films, we have used Pn as a model system for study of organic semiconducting molecules by using STM and STS. By varying tip-sample separation, different amounts of charge carriers were injected into the sample. Thereby we were able to observe transport/space charge limited tunnel current in the Pn thin films. Charge injection to empty (LUMO) and filled (HOMO) states was found to be different, with the intrinsic mobility for holes greater than that of electrons. A simple model of the charge transport process for LUMO states was used to estimate the hopping rate. We get evidence of strong charge localization at least in the vicinity of the probe-tip. Oxygen induced defect states and their influence on tunneling spectroscopy was also studied. We found amorphous like density of states signature in the normalized conductance spectra. The change in spectra is attributed to oxygen being incorporated in the Pn film with formation of some complex species of Pn molecules. Future work might involve detailed theoretical understanding of correlation of transport of charge carriers near the probe-tip to that of further away from it. This might shed light on intrinsic transport mechanisms in Pn and related materials. Also low temperature STM can be used to see temperature dependence of the spectra which would be quite useful to study intrinsic transport and thermally activated process in Pn films.

---

<sup>1</sup> Y. -E. Kim, H. Park, and J. -J. Kim, *Appl. Phys. Lett.* **69**, 599 (1996).

<sup>2</sup> S. Datta, W. Tian, S. Hong, R. Reifenberger, J. I. Henderson, and C. P. Kubiak, *Phys. Rev. Lett.* **79**, 2530 (1997).

<sup>3</sup> L. Ruppel, A. Birkner, G. Witte, c. Busse, Th. Lindner, G. Paasch, Ch. Wöll, *J. Appl. Phys.* **102**, 033708 (2007).

<sup>4</sup> S. F. Alvarado, L. Rossi, P. Müller, P. F. Seidler, W. Riess, *IBM J. Res. Dev.* **45**, 89 (2001).

<sup>5</sup> S. F. Alvarado, L. Rossi, P. Müller, and W. Riess, *Synth. Met.* **122**, 73 (2001).

<sup>6</sup> M. Kemerink, P. Offermans, J. K. J. van Duren, P. M. Koenraad, R. A. J. Janssen, H. W. M. Salemink, and J. H. Wolter, *Phys. Rev. Lett.* **88**, 096803 (2002).

<sup>7</sup> M Kemerink, S. F. Alvarado, P. Müller, P. M. Koenraad, H. W. M. Salemink, J. H. Wolter, and R. A. J. Janssen, *Phys. Rev. B* **70**, 045202 (2004).

<sup>8</sup> F. -J. Meyer Zu Heringdorf, M. C. Reuter, and R. M. Tromp, *Nature* **412**, 517 (2001).

<sup>9</sup> V. Ramachandran, M. F. Brandy, A. R. Smith, R. M. Feenstra, and D. W. Greve, *J. Electron. Mater.* **27**, 308 (1998).

- 
- <sup>10</sup> C. Baldacchini, C. Mariani, M. G. Betti, L. Gavioli, M. Fanetti, and M. Sancrotti, *Appl. Phys. Lett.* **89**, 152119 (2006).
- <sup>11</sup> Ph. Guaino, A. A. Cafolla, O. McDonald, D. Carty, G. Sheerin, and G. Hughes, *J. Phys. Cond. Mater.* **15**, S2693 (2003).
- <sup>12</sup> M. Pope, and C. E. Swenberg, *Electronic Processes in Organic Crystals and Polymers*, 2<sup>nd</sup> Edition, Oxford University Press, Oxford (1999).
- <sup>13</sup> J. Lee, S. S. Kim, K. Kim, J. H. Kim, and S. Im, *Appl. Phys. Lett.* **84**, 1701 (2004).
- <sup>14</sup> F. Amy, C. Chan, and A. Kahn, *Org. Electron.* **6**, 85 (2005).
- <sup>15</sup> M. L. Tiago, J. E. Northrup, and S. G. Louie, *Phys. Rev. B* **67**, 115212 (2003).
- <sup>16</sup> T. Yokoyama, and K. Takayanagi, *Phys. Rev. B* **61**, 5078 (2000).
- <sup>17</sup> T. Mitsui, and K. Takayanagi, *Phys. Rev. B* **62**, 16251 (2000).
- <sup>18</sup> G. Dujardin, A. J. Mayne, and F. Rose, *Phys. Rev. Lett.* **89**, 036802 (2002).
- <sup>19</sup> M. Ono, A. Kamoshida, N. Matsuura, E. Ishikawa, T. Eguchi, and Y. Hasegawa, *Phys. Rev. B* **67**, 201306(R) (2003).
- <sup>20</sup> V. Ramachandran, and R. M. Feenstra, *Phys. Rev. Lett.* **82**, 1000 (1999).
- <sup>21</sup> R. M. Feenstra, G. Meyer, and K. H. Rieder, *Phys. Rev. B* **69**, 081309 (2004).
- <sup>22</sup> M. Berthe, R. Stiuftuc, B. Grandidier, D. Deresmes, C. Delerue, and D. Stiévenard, *Science* **319**, 436 (2008).
- <sup>23</sup> A. Rose, *Phys. Rev.* **97**, 1538 (1955).
- <sup>24</sup> M. A. Lampert, and P. Mark, *Current Injection in Solids*, Academic Press (1970).
- <sup>25</sup> D. Gundlach, Y. Lin, T. Jackson, S. Nelson, and D. Schlom, *IEEE Electr. Dev. Lett.* **18**, 87 (1997).
- <sup>26</sup> M. Shtein, J. Mapel, J. B. Bensiger, and S. R. Forrest, *Appl. Phys. Lett.* **81**, 268 (2002).
- <sup>27</sup> H. Klauk, M. Halik, U. Zschieschang, G. Schmid, W. Radlik, and W. Weber, *J. Appl. Phys.* **92**, 5259 (2002).
- <sup>28</sup> T. Kelley, L. Boardman, T. Dunbar, D. Muiers, M. Pellerite, and T. Smith, *J. Phys. Chem. B* **107**, 5877 (2003).
- <sup>29</sup> X. de la Broïse, C. Delerue, M. Lannoo, B. Grandidier, and D. Stiévenard, *Phys. Rev. B* **61**, 2138 (2000).
- <sup>30</sup> M. Berthe, R. Stiuftuc, B. Grandidier, D. Deresmes, C. Delerue, and D. Stiévenard, *Science* **319**, 436 (2008).
- <sup>31</sup> E. A. Silinsh, *Organic Molecular Crystals: Their Electronic States*, Springer-Verlag (1980).
- <sup>32</sup> A. Vollmer, O. D. Jurchescu, I. Arfaoui, I. Salzmann, T. T. M. Palstra, P. Rudolf, J. Niemax, J. Pflaum, J. P. Rabe, and N. Koch, *Eur. Phys. J. E* **17**, 339 (2005).
- <sup>33</sup> J. E. Northrup, and M. L. Chabinyc, *Phys. Rev. B* **68**, 041202(R) (2003).
- <sup>34</sup> L. Tsetseris, and S. T. Pantelides, *Phys. Rev. B* **75**, 153202 (2007).
- <sup>35</sup> D. V. Lang, X. Chi, T. Siegrist, A. M. Sergent, and A. P. Ramirez, *Phys. Rev. Lett.* **93**, 086802 (2004).
- <sup>36</sup> V. Nádaždy, R. Durný, J. Puigdollers, C. Voz, S. Cheylan, and K. Gmucová, *Appl. Phys. Lett.* **90**, 092112 (2007).
- <sup>37</sup> Z. T. Zhu, J. T. Mason, R. Dieckmann, and G. G. Malliaras, *Appl. Phys. Lett.* **81**, 4643 (2002).
- <sup>38</sup> O. D. Jurchescu, J. Baas, and T. T. M. Palstra, *Appl. Phys. Lett.* **87**, 052102 (2005).